Journal of Thermal Analysis and Calorimetry, Vol. 69 (2002) 1031–1036

MICRO-THERMAL ANALYSIS OF THERMAL CONDUCTANCE DISTRIBUTION IN ADVANCED SILICON NITRIDES

J. Ye[1*], *N. Kojima*[1], *K. Furuya*[2], *F. Munakata*[2] *and A. Okada*[2]

[1]Research Department, NISSAN ARC Ltd., 1 Natsushima-cho, Yokosuka 237-0061, Japan
[2]Materials Research Laboratory, Nissan Motor Co., Ltd., 1 Natsushima-cho, Yokosuka 237-8593, Japan

Abstract

A micro-thermal analysis technique was applied to investigate advanced silicon nitride materials, which exhibit high thermal conductivity. Local thermal properties in the microstructure were evaluated, and the grain boundaries were observed to have lower thermal conductance than the Si_3N_4 grains. It was found that thermal conductance both in the grains and boundaries was lowered by the addition of the sintering aid Al_2O_3, which is soluble in Si_3N_4 grains. This indicates that high thermal conductivity in silicon nitride ceramics is achieved both by grain growth, leading to a reduction in boundary density, and by eliminating soluble elements in silicon nitride grains.

Keywords: grain boundary, local thermal conductance, μTA, Si_3N_4

Introduction

High thermal conductance in solid materials works to reduce thermal stress by homogenizing the temperature distribution. This characteristic is very important for the application of silicon nitride ceramics to mechanical and electrical components used at high temperature [1–10]. Since most ceramics, including silicon nitride, are electrical insulators and their heat transfer is governed by the phonon mode, imperfections present in the lattice greatly influence thermal conductivity. Generally, the sintering process for producing denser silicon nitride ceramics induces various imperfections into the material, leading to lower thermal conductivity ranging from 20 to 70 W m^{-1} K^{-1} [11–16]. In recent years, however, very high thermal conductivity of up to 162 W m^{-1} K^{-1} has been achieved in silicon nitride by controlling the microstructure [17]. Since both the thermal conductivity in the grains and that in the boundaries determine the overall thermal conductivity of the material, it is important to evaluate local thermal conductance corresponding to the microstructure. Micro-thermal analysis (μTA) has been used in recent years for determining the local

* Author for correspondence: E-mail: ye@nissan-arc.co.jp

1418–2874/2002/ $ 5.00

Akadémiai Kiadó, Budapest
Kluwer Academic Publishers, Dordrecht

thermal conductance, and some results have been successfully obtained for polymeric materials with low thermal conductance [18–21]. The objectives of the present study were to apply the μTA technique to silicon nitride materials having high thermal conductivity and to evaluate the local thermal properties in the microstructure.

Experimental

Two grades of silicon nitride ceramics (SN–S and SN–A) were used in this investigation. The SN–S ceramic was prepared from a powder mixture of beta Si_3N_4 powder, 1 mass% Si_3N_4 seed crystals, 1 mol% Y_2O_3 and 1 mol% Nd_2O_3. The mixed powder was die-pressed and iso-statically pressed. The powder compact was then sintered at 2473 K for 12 h under 29.4 MPa nitrogen gas to enhance grain growth. The SN-A ceramic was prepared from beta Si_3N_4 powder mixed with 2 mol% Al_2O_3 and 2 mol% Y_2O_3, and the powder compact was sintered at 2173 K for 8 h under 0.88 MPa nitrogen gas. The SN–S material was sintered at a higher temperature than the SN–A material to enhance grain growth. Laser flash measurement revealed that the thermal conductivity of the SN–S ceramic was 146 W m^{-1} K^{-1} and was much higher than that of the SN–A, which was estimated to be around 60 W m^{-1} K^{-1}. The densities of SN–S and SN–A were 3.21 and 3.23 Mg m^{-3}, respectively.

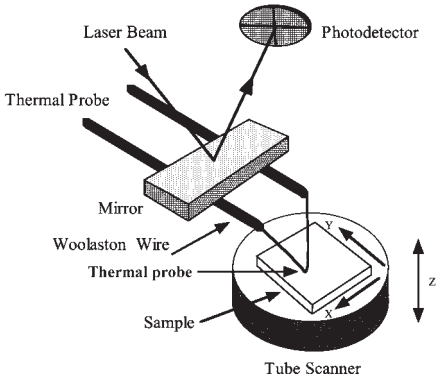

Fig. 1 Schematic diagram of a μTA microscope

Figure 1 shows a schematic diagram of a μTA microscope (μTA 2990, TA Instruments, Inc.) with a micro-differential thermal analysis (μDTA) mode for obtaining spatially resolved thermal properties corresponding to the Si_3N_4 microstructure. This equipment is based on an atomic force microscope (AFM), in which the normal probe is replaced with a wire probe with a resistive heater at the tip. In the measurement, the tip acts as a localized heater when an electric current passes through the wire, and it also works as a thermal sensor by monitoring the electric resistance of the probe. This wire tip is heated and kept at higher temperature than the specimen, so that heat can flow from the tip through the specimen when the former contacts the latter. Therefore, the thermal conduc-

tance distribution is obtained by mapping the supply power to the measuring tip at a constant temperature. Local thermal conductance, on other hand, is evaluated with the μDTA mode. In this measurement, a reference tip is kept in the air and held at the same temperature as the measuring tip that contacts the specimen. The differential supply power between the measuring tip in contact with the specimen and the reference tip in the air is calculated when the tip temperature increases from room temperature to several hundred Kelvin. In this experiment, the specimen was kept at room temperature and the spatial resolution for this method was approximately 1 micrometer. Morphology of the Si_3N_4 microstructure was observed using a tapping mode AFM. Specimens for AFM observation and μTA measurement were prepared by mechanical polishing followed by plasma etching with CF_4 gas.

Results

Figure 2 shows AFM microstructure images of the SN–S and SN–A specimens. It is clear that the SN–S specimen consists of large Si_3N_4 grains up to several tens of micrometers in diameter while the grain size of the SN–A specimen is several micrometers. Thus, heat can penetrate through the SN-S specimen with less possibility of encountering grain boundaries than in the SN–A specimen, and this agrees with the higher thermal conductivity exhibited by the SN–S ceramic. These AFM images are also consistent with scanning electron microscope observations.

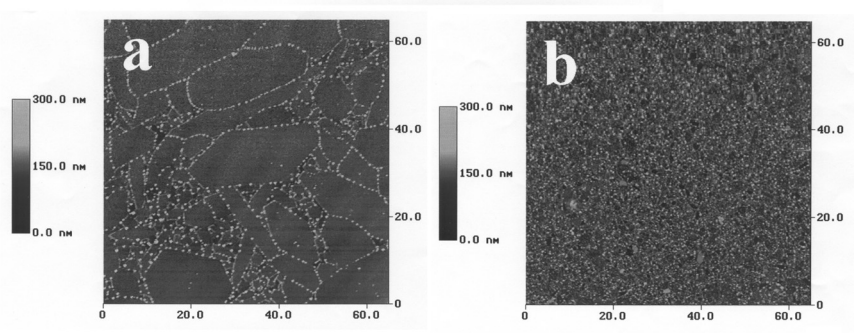

Fig. 2 AFM topographic images: a – SN–S specimen and b – SN–A specimen

Figure 3 shows thermal conductance distribution images of the SN–S and SN–A specimens. The images of the SN–S specimen are obviously consistent with the AFM microstructure images in Fig. 2a and reveal that the grain boundaries possess lower thermal conductance than the Si_3N_4 grains. As shown in Fig. 3a, b and c for tip temperatures of 373, 473, and 573 K, the difference in supply power of the measuring tip between the grains and the boundaries increases with an increase in the measuring tip temperature. Figure 3d shows the thermal conductance distribution of the SN–A specimen. It is clear that many small grains possess high thermal conductance. However, the grain boundaries between the small grains are unclear in comparison with the images in Figs 3a–c due to the limited spatial resolution of approximately one mi-

crometer. Nevertheless, some small dark areas with low conductance are observed, and these areas are thought to correspond to the multigrain junction boundaries among several small grains [16, 22].

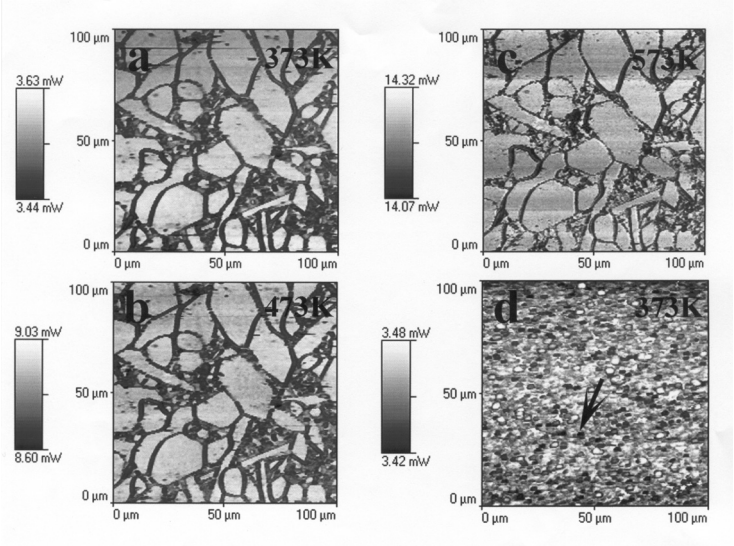

Fig. 3 Thermal conductance distributions determined by µTA: a–c – the SN–S specimen at tip temperatures of 373, 473, and 573 K, respectively, and d – the SN–A specimen at a tip temperature of 373 K. The dark area indicated by the arrow is a multigrain junction boundary

Figure 4 shows µDTA profiles obtained at the Si_3N_4 grains and grain boundaries of the SN–S and SN–A specimens. The boundary in the SN-A specimen corresponds to the small dark area seen in Fig. 3d. The profiles indicate the differential supply power between the measuring and reference tips as a function of the tip temperature, which ranges from 350 to 550 K. It is observed that the supply power for both the grains and boundaries of the SN–S specimen is higher than that of the SN–A specimen and increases more abruptly with an increase in the tip temperature. Thus, it is concluded that the grains and boundaries in the SN–S specimen have higher thermal conductance than those in the SN–A specimen.

Discussion

Oxide additives for sintering Si_3N_4 have been reported to form two types of silicate-based amorphous phase: a two-grain junction boundary and a multigrain junction boundary [16, 22]. The former boundary is a thin film formed between two Si_3N_4 grains, and its thickness is approximately 1 nm in any given material. The latter boundary is surrounded by three or more Si_3N_4 grains, and its size ranges from 0.1 to 1 µm. It might be difficult to determine the local thermal conductance at the boundary

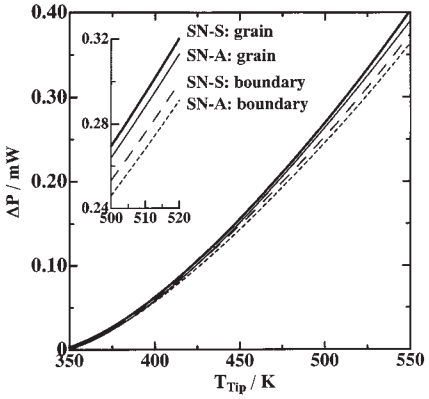

Fig. 4 Comparison of μDTA profiles obtained at the Si_3N_4 grains and grain boundaries of the SN–S and SN–A specimens. The differential supply power ΔP is plotted as a function of the tip temperature T_{Tip}

accurately due to the limited spatial resolution of the μTA microscope of just 1 μm. In this investigation, boundaries with lower thermal conductance than the grains are2 clearly observed in Fig. 3. The measured boundary area is around 1–2 μm in width, which is much greater than the real thickness of the grain boundaries. This indicates that local thermal conductance around the boundaries is measured as the value of the boundaries, and that the measured difference in thermal conductance between the amorphous boundary phase and the Si_3N_4 grains is much smaller than the actual difference. It also suggests that further work is required for determining the local thermal properties at the grain boundaries of silicon nitrides in detail. Actually, in this study, clear μTA images were obtained in spite of the small measured difference in thermal conductance between the boundaries and the grains.

Al ions are known to dissolve in Si_3N_4 materials to form a solid solution, so-called sialon, expressed by the formula $Si_{6-z}Al_zO_z\ N_{8-z}$ (z=0–4). The μDTA profiles shown in Fig. 4 reveal that the thermal conductance values are low both in the Si_3N_4 grains and boundaries of the SN–A specimen, in comparison with those of the SN–S specimen. This suggests that Al and O ions dissolve not only into the Si_3N_4 grains but also into the grain boundaries, which could account for the lower thermal conductance of the SN–A specimen.

Conclusions

Grain boundaries in silicon nitride were confirmed to possess considerably lower thermal conductance than the grains, and the addition of Al_2O_3 to silicon nitride as a sintering aid reduced the thermal conductivity of silicon nitride. Therefore, thermal conductivity in silicon nitride ceramics is enhanced by grain growth that reduces the boundary density and by eliminating foreign soluble elements, such as Al and O ions, in silicon nitride grains.

* * *

This work has been supported by the New Energy and Industrial Technology Development Organization (NEDO) as part of the Synergy Ceramics Project under the Industrial Science and Technology Frontier (ISFT) program promoted by the National Institute of Advanced Science and Technology (AIST) under the Ministry of Economy, Trade and Industry (METI) of Japan.

References

1 D. R. Johnson, A. C. Schaffhauser, V. J. Tennery and E. L. Long, Jr., Am. Ceram. Soc. Bull., 64 (1985) 276.
2 H. Takao, A. Okada, M. Ando, Y. Akimune and H. Hirosaki, Proc. of 4th International Symposium on Ceramic Materials and Components for Engines, Ed. by R. Carlson, T. Johansson and L. Kahlman, Elsevier Applied Science, London 1992, p. 118.
3 H. Kawamura, Proc. of 6th International Symposium on Ceramic Materials and Components for Engines, Ed. by K. Niihara, S. Kanzaki, K. Komeya, S. Hirano and K. Morinaga, Japan Fine Ceramics Association, Tokyo 1998. p. 5.
4 M. J. Hoffmann and G. Petzow, Tailoring of Mechanical Properties of Si_3N_4 Ceramics, Kluwer, Dordrecht 1994, p. 403.
5 S. K. Ghandhi, VLSI Fabrication Principles, Wiley, New York 1983, p. 427.
6 J. J. Chang, Proc. IEEE, 64 (1976) 1039.
7 I. Shimizu, J. Non-Cryst. Solids, 78 (1985) 1363.
8 M. J. Powell, B. C. Easton and O. F. Hill, Appl. Phys. Lett., 38 (1981) 794.
9 A. R. Zanatta and L. A. O. Nunes, Appl. Phys. Lett., 72 (1998) 3127.
10 H. Sunamura, T. Sakamoto, Y. Nakamura, H. Kawaura, J. S. Tsai and T. Baba, J. Appl. Phys., 74 (1999) 3555.
11 T. Hirai, S. Hayashi and K. Niihara, Am. Ceram. Soc. Bull., 57 (1978) 1126.
12 G. Ziegler, Progress in Nitrogen Ceramics, Ed. by F. L. Riley, Martinus Nijhoff Boston, MA, 1983.
13 K. Hayashi, S. Tsujimoto, T. Nishikawa and Y. Imamura, Yogyo-Kyokai-shi, 94 (1986) 595.
14 K. Watari, Y. Seki and K. Ishizaki, J. Ceram. Soc. Jpn., 97 (1989) 56.
15 K. Watari, K. Ishizaki and K. Mori, J. Am. Ceram. Soc., 74 (1991) 244.
16 N. Hirosaki, Y. Okamoto, M. Ando, F. Munakata and Y. Akimune, J. Am. Ceram. Soc., 79 (1996) 2878.
17 Y. Akimune, F. Munakata, K. Matsuo, N. Hirosaki, Y. Okamoto and K. Misono, J. Ceram. Soc. Jpn., 107 (1999) 107.
18 M. Reading, Trends Poly. Sci., 1 (1993) 248.
19 M. Song, A. Hammiche, H. M. Pollock, D. J. Hourston and M. Reading, Polymer, 37 (1996) 5661.
20 D. J. Hourston, M. Song, A. Hammiche, H. M. Pollock and M. Reading, Polymer, 38 (1997) 1.
21 M. Song, H. M. Pollock, A. Hammiche, D. J. Hourston and M. Reading, Polymer, 38 (1997) 503.
22 H. J. Kleebe, M. K. Cinibulk, R. M. Cannon and M. Ruhle, J. Am. Ceram. Soc., 76 (1993) 1969.